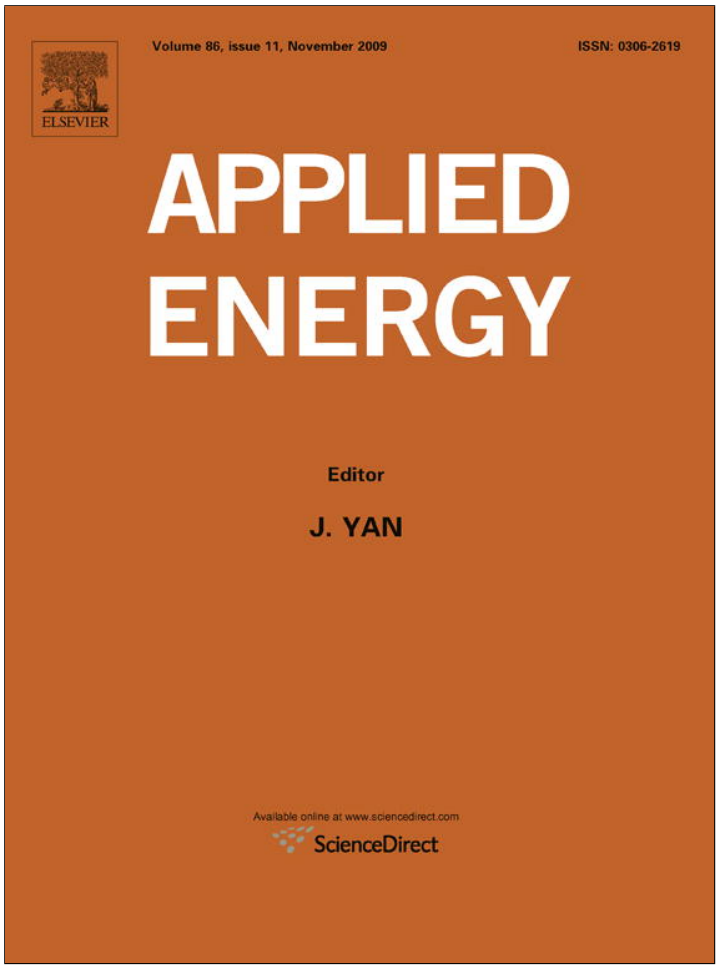

Applied Energy 86 (2009) 2466–2475

Contents lists available at ScienceDirect

Applied Energy

journal homepage: www.elsevier.com/locate/apenergy

Analysis of biogas compression system dynamics

Mirko Morini *, Michele Pinelli, Mauro Venturini

ENDIF – Engineering Department in Ferrara, University of Ferrara, Via Saragat, 1 – 44100 Ferrara, Italy

ARTICLE INFO

Article history:
Received 6 October 2008
Received in revised form 4 March 2009
Accepted 5 March 2009
Available online 7 April 2009

Keywords:
Compression
Dynamics
Surge
Natural gas
Biogas
Hydrogen

ABSTRACT

The use of biogas for energy production has progressively increased in recent years, due to an increasing interest both in agricultural and energy policies of many industrialized countries. Biogas compression by means of natural gas infrastructure seems the most immediate solution, but could also lead to problems due to the different physical properties of the two gases. In this paper, a non-linear one-dimensional modular dynamic model is developed and used for the simulation of compression system transient behavior. The arrangement consists of a main line, where the compressor operates, and an anti-surge control, which consists of a recycle loop activated by a fast acting valve. Different maneuvers (start-up, normal operation, emergency shutdown and operating point variation) are simulated by using two different working fluids (methane and biogas). Simulations prove that the design of the surge protection system should consider the fluid to be elaborated. Moreover, system predisposition to surge increases as the ratio between system volumes and the inertia of the rotating masses increases.

1. Introduction

The use of biogas for energy production has progressively increased in recent years, due to an increasing interest both in agricultural and energy policies of many industrialized countries.

At present, the exploitation of biomass resources is considered as a viable addition with respect to the use of fossil fuels and so a great deal of research is directed towards investigating the effective capabilities of such resources [1]. Moreover, biogas is a predictable renewable energy source. This is very important in distributed grid-connected generation where unpredictable renewable energy sources, like solar photo-voltaic and wind, have proved to be critical for network voltage and frequency stability [2,3].

In order to use biogas as fuel for energy production, the gas has to be compressed up to the feeding pressure of the energy system. Moreover, also in the case of biogas injection into the natural gas distribution grid, biogas pressure has to be raised.

Therefore, the use of natural gas infrastructure seems the most immediate solution for biogas compression, but could also lead to problems due to the different physical properties of the two gases.

In fact, one of the key problems is surge, which is a compressor instability characterized by a variation in time of the pressure ratio and of the mass flow rate. The onset in the most severe form, known as deep surge, can lead to severe damage due to the inversion of the mass flow rate [4,5]. Moreover, surge is one of the major limiting factors of the compressor operating range, performance and reliability. It occurs at operating points with low mass flow rate and high pressure ratio. The line connecting the points where surge occurs at the various rotational speeds is named "surge line".

For these reasons, different strategies to avoid compressor operation beyond the surge line have been developed and can be grouped into three categories:

- surge detection, through the precursors of instabilities, which requires large control forces and very fast actuators [6–9];
- surge avoidance, based on the definition of a surge avoidance line, which is conservative if compared to the surge line. The definition of the surge avoidance line does not allow the compressor to operate close to the surge line, i.e. in the maximum efficiency region [10];
- surge control, by shifting the surge line towards lower mass flow rates and higher pressure ratios. Surge control can be operated by means of active tools (e.g. close coupled valves, air or water injection and bleed valves) [11–14] or by means of passive tools (e.g. casing treatments, variable guide vanes, movable plenum walls, bouncing balls) [15,16].

Since the set up of these strategies by means of an experimental campaign can be expensive, many papers based on modeling turbomachine behavior are presented in literature.

Two of the most successful models for simulating compressor instabilities are the Greitzer model [4] and the Moore and Greitzer (MG) model [17], which have been widely adopted by many authors in literature both to study compressor instabilities and to set up devices to avoid compressor operation beyond the surge line.

* Corresponding author. Tel.: +39 (0)532 974966; fax: +39 (0)532 974880.
E-mail address: mirko.morini@unife.it (M. Morini).

0306-2619/$ - see front matter © 2009 Elsevier Ltd. All rights reserved.
doi:10.1016/j.apenergy.2009.03.008

Nomenclature

A	area
B_t	body configuration
B	body
C	compressor, torque
c	torque per unit mass
c_p	specific heat at constant pressure
D_h	hydraulic mean diameter
e	PID input
ED	exhaust duct
f	force per unit mass
$\mathbf{I}$	identity matrix
ID	intake duct
J	polar inertia
k	ratio of specific heats
K_p	PID proportional gain
K_V	valve coefficient
L	length
LHV	lower heating value
M	$\pi R^2 L\rho$ cylinder mass
$\boldsymbol{n}$	external normal versor
n_r	$\frac{2\pi}{60}\frac{\omega}{\sqrt{T_3}}$ corrected rotational speed
p	pressure
P	point, power
r	radial coordinate
R	radius, gas constant
SAL	surge avoidance line
SM	surge margin
SOP	stationary operating point
t	time
T	temperature
T_d	PID derivative time
T_i	PID integral time
u	PID output
$\boldsymbol{v}$	Eulerian velocity
V_{acc}	access valve
V_{out}	outlet valve
V_{rec}	recycle valve
x	curvilinear coordinate
w	mass flow rate
w_r	$=\frac{w_4\sqrt{RT_4}}{p_4}$ corrected mass flow rate
β	$=\frac{p_4}{p_3}$ pressure ratio
η	efficiency
θ	tangential coordinate
λ	friction factor
ρ	density
τ	time
$\boldsymbol{\varphi}$, $\boldsymbol{\Phi}$	flux
ψ	generic intensive property
$\boldsymbol{\Psi}$	energy delivery index
ω	angular speed
$\boldsymbol{\Gamma}$	viscous stress tensor
Ω	solid cylinder

Subscripts and superscripts

0,...,9	model sections
a	absorbed
acc	access
amb	ambient
C	compressor
ED	exhaust duct
f	final, friction
i	initial
ID	intake duct
pm	power dwell
pr	power rise
ps	power trip
out	outlet
r	radial
RD	recycle duct
rec	recycle
rf	reverse flow
s	supplied
SL	surge line
t	time
vm	valve dwell
vps	valve pre-stroke
vs	valve stroke
θ	tangential

Concerning compressor instabilities, the MG model has been applied in [18] to study surge effects on a turbocharger compressor, while a control-theoretic form of the MG model and a Liapounov stability analysis of rotating stall and surge were presented in [19]. The MG model was also adopted to perform bifurcational analyses (see for instance [20–22]). A non-linear control law for active stall/surge controllers was derived in Ref. [23]. In Ref. [24] higher order Galerkin expansion of the MG model was investigated.

A great number of papers have also been published to address the problem of developing compressor control devices, for which the MG model was widely used. In Ref. [11] the use of pulsed air injection to control rotating stall in low speed axial flow compressors was presented and jet injection with a high order Galerkin method was studied in Ref. [25]. In Ref. [26], a close coupled valve for surge and rotating stall control was presented. In Refs. [15,27] a control device based on the aeroelastic coupling of the basic compression system with a hydraulic oscillator was illustrated. In Ref. [13], the MG model was applied to a system in which wet compression was used for active control of compression system instabilities.

Other successful models, which allow the simulation of compressor instabilities and mainly used for aeronautic applications, are the DYNTECC model (DYNamic Turbine Engine Compressor Code) [28] and the ATEC model (Aerodynamic Turbine Engine Code), which extended the DYNTECC model to consider the whole gas turbine [29,30]. In particular, the DYNTECC model was applied to study axial–centrifugal compressors off-design behavior [31,32].

Many other models can be found in literature. For instance, interesting models, which simulate the transient behavior of turbocharger compressors in diesel engines and also the compressor surging and its emergency shutdown, are developed in Refs. [33–35]. In Ref. [36], a model was applied to a closed loop Brayton Cycle. Effects of surge on a hybrid system (Solid Oxide Fuel Cell and Gas Turbine) were also studied in Refs. [37,38].

Another important field where models have been used is the simulation of natural gas compression stations since forced stops can result in significant economic losses. Different models [10,39–44] have been presented in literature dealing with modeling compression systems and set up of surge avoidance strategies. In Ref. [39], a model was developed and applied to three test cases: a compressor surge protection control, a compressor start-up for a single unit compressor station and a compressor station set point change for a compressor station composed of two compressors in series. In Ref. [40] the compressor deceleration during shutdown and the effects of recycle coolers on compressor surge were studied

for a single unit compression station. Transient phenomena associated with gas recycling during compressor emergency shutdown have been studied both experimentally and numerically in Ref. [41]. Some general conclusions have been drawn: (i) the recycle valve pre-stroke time is more important than the stroke time and it should be made as short as possible and (ii) the recycle valve should be located as close as possible to the compressor (no matter if it is near the suction side or the discharge side) [40,41]. Similar rules of thumb are expressed in Ref. [10]. A parametric study on a compressor station composed of five multistage centrifugal compressors in parallel was carried out in Refs. [42,43].

In this paper, a non-linear one-dimensional modular dynamic model, implemented through a physics-based approach, is developed and used for the simulation of compressor transient behavior. The arrangement consists of a main line, where the compressor operates, and an anti-surge control, which consists of a recycle loop activated by a fast acting valve when the control system detects the crossing of the surge avoidance line. This is a widely employed device for surge avoidance in compression stations [10].

The arrangement for the compression station was derived from one of the configurations adopted in Ref. [41]. The compression station is composed of a main flow line and of a recycle line, which acts as an anti-surge system to ensure a proper surge margin during normal operation.

Two different working fluids (methane and biogas) and two different values of surge margin (10% and 20% with respect to the surge line, for a given rotational speed) are considered. Moreover, the presence of a cooler along the main flow line is analyzed and discussed.

Three maneuvers are simulated:

- compressor behavior from start-up to normal operation;
- emergency shutdown. In this case, the analysis of the influence of the motor polar inertia is also evaluated;
- operating point variation, through a reduction of the mass flow rate at compression system outlet.

Surge occurrence is evaluated for all cases. Moreover, a PID controller is set up and tuned to increase compression system stability towards surge.

2. Model development

2.1. General balance equation

The development of the mathematical model to determine the laws of conservation (mass, momentum and energy) is carried out starting from a general approach.

The main features which characterize the model developed in the current paper are:

- this model is based on formulas for each material point, differently from other models in literature which are based on integral formulas [45];
- use of finite difference method instead of a lumped parameter method. This allows the one-dimensional discretization of the problem. For instance, one or more elements may be adopted to represent each single component;
- modularity, so that every system configuration can be represented by means of basic components (valve, duct and compressor);
- use of dimensional quantities, which allows an easy-to-read analysis of the results, both in terms of physical interpretation and of practical quantification.

Let us consider a generic scalar intensive property

$$\psi = \psi(\boldsymbol{x}, t) \tag{1}$$

defined for $\boldsymbol{x} \in B_t$, where B_t is the configuration of a generic body B at time t.

By using an Eulerian approach, the rate of variation of the property expressed through the substantial derivative over a finite volume $S_t \subset B_t$ can be written as

$$\frac{D}{Dt}\int_{S_t} \psi(\boldsymbol{x}, t) d\Omega \tag{2}$$

where $d\Omega$ is the infinitesimal element of volume.

This variation can be assumed [46] equal to the sum of two general contributions:

- a flux term, written as

$$-\int_{\partial S_t} \boldsymbol{\varphi} \cdot \boldsymbol{n} d\sigma \tag{3}$$

where $\boldsymbol{\varphi}$ is the flux vector, $d\sigma$ is the infinitesimal element of area and $\boldsymbol{n}$ is the external normal versor to boundary surface ∂S_t (the minus sign in Eq. (3) is due to the versus of normal versor);

- a source term

$$\int_{S_t} \rho r d\Omega \tag{4}$$

where r is the property generated per unit mass and per unit time and ρ is the density. Hence, property balance equation can be written as

$$\frac{D}{Dt}\int_{S_t} \psi(\boldsymbol{x}, t) d\Omega = -\int_{\partial S_t} \boldsymbol{\varphi} \cdot \boldsymbol{n} d\sigma + \int_{S_t} \rho r d\Omega \tag{5}$$

The Transport Theorem can be applied to the first member of Eq. (5) and the Divergence Theorem to the first term of the second member. Since Eq. (5) is valid for any $S_t \subset B_t$ and by assuming the continuity of the integral arguments, the balance equation can be written for any $\boldsymbol{x} \in B_t$ as:

$$\frac{D\psi}{Dt} + \psi \nabla \cdot \boldsymbol{v} = -\nabla \cdot \boldsymbol{\varphi} + \rho r \tag{6}$$

where $\boldsymbol{v}$ is the Eulerian velocity.

By using the definition of the substantial derivative, Eq. (6) can be reformulated as

$$\frac{\partial \psi}{\partial t} + \nabla \cdot (\psi \boldsymbol{v}) = \nabla \cdot \boldsymbol{\varphi} + \rho r \tag{7}$$

For a vectorial intensive property $\boldsymbol{\psi} = \boldsymbol{\psi}(\boldsymbol{x}, t)$, by assuming that the flux through the boundary and the source term can be written as $\boldsymbol{\Phi n}$ and $\rho \boldsymbol{r}$, respectively, the balance equation for any $\boldsymbol{x} \in B_t$ is

$$\frac{\partial \boldsymbol{\psi}}{\partial t} + \nabla \cdot (\boldsymbol{v}^T \boldsymbol{\psi}) = \nabla \cdot \boldsymbol{\Phi} + \rho \boldsymbol{r} \tag{8}$$

2.2. Continuity equation for fluids

In this case, the scalar property is the density distribution $\rho = \rho(\boldsymbol{x}, t)$. By assuming the validity of the Conservation of Mass Principle the source term is null. Moreover, any configuration S_t is composed of the same points (independent of time t), so the flux term is null too.

For a one-dimensional system, density is a function of the curvilinear coordinate x and time and Eq. (7) is reduced to

$$\frac{\partial \rho}{\partial t} + \frac{\partial \rho v}{\partial x} = 0 \tag{9}$$

Moreover, let us consider a duct whose length is L and whose area is $A(x)$ and which is normal to the curvilinear abscissa x. Fluid properties can be assumed constant on each section and only variable with respect to the curvilinear abscissa.

By denoting with the subscripts "i" and "f" the initial and final sections of the L-length duct, respectively, and by expressing Taylor series with Peano remainder of the function ρv (remainders can be neglected), Eq. (9) can be written for these two sections as

$$\frac{\partial p_{i,f}}{\partial t} = \frac{kRT_{i,f}}{A_i A_f} \cdot \frac{A_f w_i - A_i w_f}{L} \tag{10}$$

2.3. Momentum balance for fluids

In this case the vectorial property is the momentum $\rho(\boldsymbol{x},t)\boldsymbol{v}(\boldsymbol{x},t)$. By noting that for a fluid in motion the stress tensor $\boldsymbol{\Phi}$ is equal to $(-p\mathbf{I}+\boldsymbol{\Gamma})$ and the source term $\boldsymbol{r}$ is equal to the vectorial sum of forces per unit mass working on the fluid, Eq. (8) can be reformulated as

$$\frac{\partial \rho \boldsymbol{v}}{\partial t} + \nabla \cdot (\rho \boldsymbol{v}^T \boldsymbol{v}) = -\nabla \cdot (p\mathbf{I} + \boldsymbol{\Gamma}) + \rho \sum \mathbf{f} \tag{11}$$

By considering a one-dimensional system, as in the previous paragraph, by taking into account the viscous stress tensor by means of the friction factor and by neglecting body forces (such as gravity), and by assuming that the kinetic energy of the fluid and its variation can both be neglected, Eq. (11) can be written for the initial and final section as

$$\frac{\partial w_{i,f}}{\partial t} = -\frac{A_{i,f}}{L}(p_f - p_i) - \frac{\lambda_{i,f}}{D_{hi,f}} \frac{RT_{i,f}}{A_{i,f} p_{i,f}} \frac{w_{i,f}^2}{2} \tag{12}$$

where as in the previous paragraph, the pressure for the initial and final section can be expressed through the Taylor series with Peano remainder retained up to the first order.

2.4. Momentum balance for rotating masses (spool dynamics)

Let us consider a solid cylinder (length L and radius R) rotating around its axis with angular velocity ω.

By assuming pressure and shear stresses on the boundary surface to be negligible and by using cylindrical coordinates (r,θ,z), it is possible to write

$$v_\theta = \omega r \quad \forall P \in \Omega \tag{13a}$$
$$v_r = 0 \quad \forall P \in \Omega \tag{13b}$$
$$v_z = 0 \quad \forall P \in \Omega \tag{13c}$$
$$\boldsymbol{\Phi} = 0 \quad \forall P \in \Omega \tag{13d}$$

By adopting cylindrical coordinates, Eq. (8) for the momentum can be written for any point of the cylinder through the following scalar equation:

$$\frac{\partial \rho \omega r}{\partial t} + \frac{1}{r}\frac{\partial \rho \omega^2 r^2}{\partial \theta} = \rho f_\theta \tag{14}$$

where f_θ is the resultant in θ direction of the forces per unit mass. Let us assume a homogenous density for the cylinder and let us note that angular velocity and radius are independent of the tangential coordinate. By defining the torque per unit mass as $c = 2f_\theta r$, by integrating over the cylinder volume and by applying the Integral Mean Value Theorem to the second member, it is possible to obtain

$$J\frac{\partial \omega}{\partial t} = C \tag{15}$$

where C is the resultant of the torques applied to the cylinder and $J = MR^2$.

This latter equation can be written in terms of power P as follows:

$$J\frac{\partial \omega}{\partial t} = \frac{P}{\omega} \tag{16}$$

3. Model implementation

A sketch of the system under consideration is presented in Fig. 1. The system is composed of a main line, where the compressor operates, and a recycle line. In the recycle line, the valve V_{rec} allows compressor normal operation within the imposed surge margin. In case of an emergency shutdown (ESD), the valve can also protect the system.

Model equations are written for nine control sections as depicted in Fig. 2. Six continuity equations, as Eq. (10), are written for sections 0, 2, 3, 4, 6 and 9 while five momentum balance equations, as Eq. (12), are written for sections 1, 3, 5, 7 and 8. The spool dynamics is represented by Eq. (17).

$$J\frac{\partial \omega}{\partial t} = \frac{P_s - P_a - P_f}{\omega} \tag{17}$$

The power supplied P_s is an input of the system, while the power absorbed by the compressor P_a is calculated in the case of direct flow by using the following expression:

$$P_a = w_2 c_p T_1 \left(\left(\frac{p_2}{p_1} \right)^{\frac{k-1}{k\eta}} - 1 \right) \tag{18}$$

where η is the isentropic efficiency calculated by using the experimental maps.

According to [12], a centrifugal compressor where reverse flow is present can be approximated to a turbine. In this model, this hypothesis is assumed valid even for an axial–centrifugal compressor. Hence, in the case of reverse flow, the absorbed power P_a can be calculated as

$$P_a = w_2 c_p T_2 \left(\left(\frac{p_1}{p_2} \right)^{\frac{\eta_{rf}(k-1)}{k}} - 1 \right) \tag{19}$$

where η_{rf} is the value of efficiency assumed equal to 0.1.

The friction power P_f can be estimated through a second degree polynomial function of compressor rotational speed, fitted over experimental data.

In all equations, as previously outlined, temperature is considered and it represents a fundamental variable of the model. The compressor outlet temperature is estimated through the polytropic efficiency derived by using experimental maps. Moreover, the specific heat at constant pressure depends on temperatures through fourth grade polynomials. The coefficients of the polynomial are different for each working fluid. This implies that the specific heat

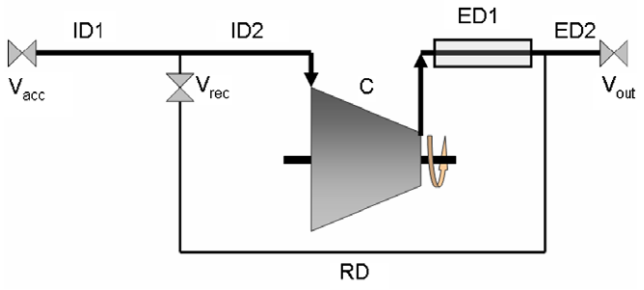

Fig. 1. Schematic representation of the compression system.

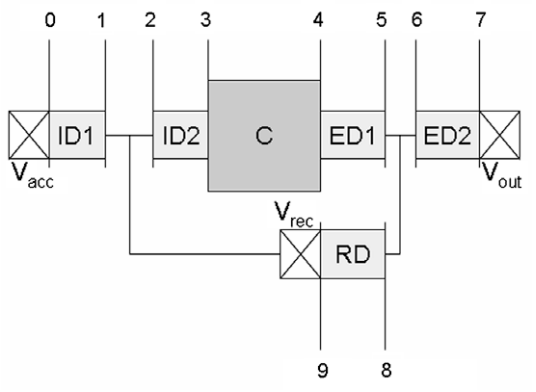

Fig. 2. Model of the system.

ratio k is calculated by taking into account actual temperatures and working fluid.

Valves are simulated through Eqs. (20)–(22).

$$w_0 = \mathrm{sign}(p_{amb} - p_0) \cdot K_{Vacc} \sqrt{\rho_{amb} \cdot |p_{amb} - p_0|} \tag{20}$$

$$w_9 = \mathrm{sign}(p_9 - p_2) \cdot K_{Vrec} \sqrt{\rho_9 \cdot |p_9 - p_2|} \tag{21}$$

$$p_7 = p_{amb} + \frac{w_7 |w_7|}{\rho_7 \cdot K_{Vout}^2} \tag{22}$$

In this application, the nominal value of each parameter required by the model has been chosen either following the values reported in [41] or by using ad hoc values. The parameter values are reported in Table 1.

3.1. Compressor characteristic curves

Compressor characteristic curves are implemented in the model in the form suggested by Koff and Greitzer [47] for the unstable characteristic and in a second degree polynomial form fitted over experimental data for the stable characteristic curve (Fig. 3). Compressor outlet mass flow rate w_4 is calculated by means of this type of characteristic curves.

3.2. Solver

To solve the system of ordinary differential equations, a fifth order Runge–Kutta method with a fourth order error control is used.

Table 1
Model input parameters.

Property	Value	Unit	Ref.
Main line			
Hydraulic diameters, D_{hi} ($i = 1,\ldots,7$)	0.08	m	[41]
Intake duct length, L_{ID1}	60	m	[41]
Intake duct length, L_{ID2}	1.5	m	[41]
Exhaust duct length, L_{ED1}	19	m	[41]
Exhaust duct length, L_{ED2}	60	m	[41]
Compressor duct length, L_C	0.40	m	[44]
Friction factors λ_1, λ_3, λ_5, λ_7	0.01	–	
Access valve coefficient, $K_{Vacc} \times 10^3$	5	m^2	
Outlet valve coefficient, $K_{Vout} \times 10^3$	5	m^2	
Recycle line			
Hydraulic diameter, D_{hi} (i = 8,9)	0.04	m	[41]
Recycle duct length, L_{RD}	16	m	[41]
Friction factor, λ_8	0.01	–	
Maximum recycle valve coefficient, $K_{Vrec} \cdot 10^3$	1	m^2	
Ambient pressure, p_{amb}	101	kPa	
Ambient temperature, T_{amb}	15	°C	
Inertia, J	0.1	kg m^2	[44]
Maximum power supplied, P_s	50	kW	

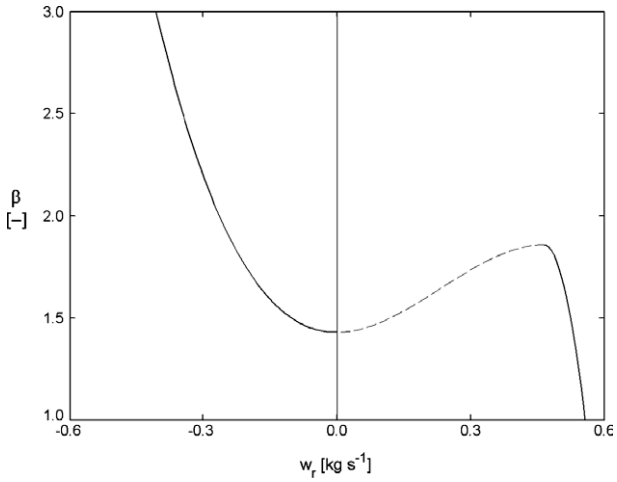

Fig. 3. Characteristic curves used for compressor behavior simulation in stable and unstable regions – n_r = 29,808 rpm.

This method is implemented as a variable-step solver, which is named ODE45 and is supplied with Matlab®. For the simulations, five ODE45 parameters have been set: maximum, minimum and initial step size as well as relative and absolute tolerance. The maximum step size and the relative tolerance have been set equal to 0.1 s and 0.1%, respectively, while the rest has been set to "auto".

4. Results and discussion

The model described in the previous section is applied to evaluate whether the plant configuration under study allows compressor operation within a given surge margin.

The surge margin is commonly quantified by using two definitions. In industrial applications, it accounts for the distance between the actual operating point and the surge point at a constant corrected mass flow rate. On the other hand, surge margin, as defined by NASA, measures the distance between the operating point and the surge point in terms of compressor pressure ratio at constant corrected speed. NASA definition accounts for throttle area changes representing the equivalent throttling process required to take the compressor into stall [48]. Moreover, such a definition does not require the use of mass flow rate, which can be usually determined with more difficulty and with a higher uncertainty than corrected rotational speed. For these reasons, the surge margin definition adopted for the simulations is the following:

$$SM = \left. \frac{\beta_{SL} - \beta}{\beta_{SL}} \right|_{n_r} \tag{23}$$

Two values of surge margin, 10% and 20%, are considered and thus two surge avoidance lines (*SAL*) are identified.

The valve is controlled through a PID controller. The input of PID $e(t)$ is the difference between the actual value of the compressor pressure ratio and the correspondent value on the surge avoidance line. The output $u(t)$ is used to identify valve position: if $u(t)$ is positive the valve opens; otherwise, it closes.

$$u(t) = K_p \left(e(t) + \frac{1}{T_i} \int_0^t e(\tau) d\tau + T_d \frac{de(t)}{dt} \right) \tag{24}$$

The initial values of PID controller parameters, were chosen according to classical Ziegler–Nichols methods [49]. Then, PID fine tuning was performed step-by-step, by means of a trial-and-error procedure. Final values of PID controller parameters are summarized in Table 2.

Two working fluids are considered for the simulations carried out. The first one is pure methane, while the second one is a mixture of methane and carbon dioxide (60% CH_4 and 40% CO_2 on a volume basis). This composition can be considered representative of the gas obtainable by means of biochemical conversion processes, as for instance, the anaerobic digestion [50]. This gas will be identified in the text as biogas. Mixtures with a composition close to that of biogas are becoming very widespread for distributed power generation. Thus, particular attention has to be focused on the problems which may arise when such gases are compressed by using the compression stations and the pipelines adopted for natural gas.

Moreover, the same compression system configuration is also used to simulate the behavior of a compression station which elaborates a CH_4–H_2 mixture composed of 90% methane and 10% hydrogen on a volume basis. Mixtures composed of methane and hydrogen are of particular interest and so the impact of hydrogen injection on compressor performance should also be evaluated. In fact, the effect of hydrogen addiction to natural gas is mainly investigated with reference to steel for transmission pipes, to polymer materials for distribution pipes, to valves and to domestic gas meters [51]. At present, effects on compressors are not considered since the injection is performed in the medium pressure grid (where gas pressure passes from 40 bar to 8 bar), i.e. after the main compression stations. Therefore, although the main compression stations are not involved, the CH_4–H_2 mixture could pass through booster compressors.

Since a preliminary analysis showed that the dynamic behavior of the CH_4–H_2 mixture is almost the same as that of pure methane, the results of the dynamic simulation for this mixture will not be reported in the following. In fact, this mixture will be used to compare the overall compression system performance when different fluids are elaborated under stationary conditions, as summarized in Table 3.

4.1. Surge avoidance during start-up and normal operation

For this analysis, the recycle line is used to ensure proper surge margin during compressor start-up and normal operation. The results of this analysis are shown in Fig. 4. It can be noticed that, by using methane as the working fluid, the system cannot guarantee the 20% *SM* condition (thin black line), while it ensures safe operation in case of *SM* = 10% (thick black line). By using biogas, the system allows compressor safe operation for both *SM* values (10% thick gray line and 20% thin gray line). This can be explained by considering that methane has a lower density than biogas and so, according to Eq. (21), a lower mass flow rate passes through the recycle valve.

Table 2
PID controller parameters.

		Value
Proportional gain	K_p	−0.1
Integral time	T_i	100
Derivative time	T_d	0.1

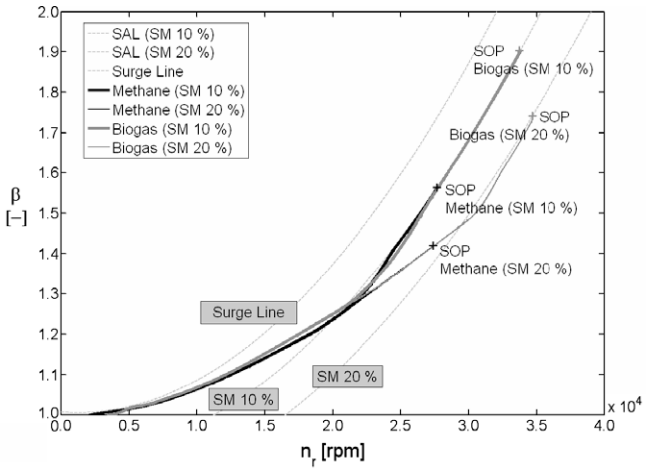

Fig. 4. Surge avoidance during start-up and normal operation.

Behavior-in-time of the recycle valve coefficient K_{Vrec} is presented in Fig. 5. The trend corroborates the above-mentioned consideration. In fact, when methane is used as the working fluid, K_{Vrec} is always higher than in the case of biogas for a fixed *SM* value. In particular, K_{Vrec} reaches its maximum value, i.e. the valve is completely open, when a *SM* = 20% is requested.

The results of the simulations for the three considered fluids (methane, biogas and CH_4–H_2 mixture) are summarized in Table 3 in order to evaluate overall compression system performance under stationary conditions in the case of *SM* = 10%.

It can be observed that the valve opening is required to be larger in the case of the CH_4–H_2 mixture than in the case of methane to ensure the same surge margin. This implies that, when the CH_4–H_2 mixture is used instead of methane, the protection margin of the anti-surge system is lower.

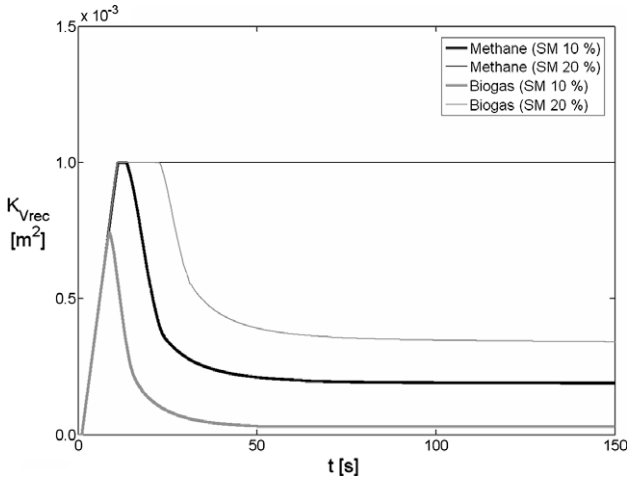

Fig. 5. Recycle valve coefficient during start-up and normal operation for different working fluids and surge margin.

Table 3
Compression system performance.

	$K_{Vrec} \times 10^3$ (m^2)	w_7 (kg/s)	*LHV* (kJ/kg)	P_S (kW)	Ψ (–)	β (–)
Methane	0.190	0.247	49942	50.0	247	1.56
Biogas	0.036	0.371	17653	50.0	131	1.90
CH_4–H_2 mixture	0.233	0.228	50906	50.0	232	1.51

Another consideration, dealing with energy fluxes through a compression station, can be drawn. An energy delivery index Ψ can be defined as in Eq. (25) to relate the compression station outlet energy delivery to the power supplied for compressing the gas.

$$\Psi = \frac{w_7 \cdot LHV}{P_S} \tag{25}$$

It can be highlighted that the mass flow rate at the compression system outlet w_7 decreases by adding hydrogen to methane. Moreover, the energy delivery index Ψ for CH_4–H_2 mixture is lower than for methane, i.e. a higher power is required to provide the same energy delivery to the distribution grid, even though the *LHV* value is higher. Finally, the biogas provides the lowest Ψ value, mainly due to the fact that biogas *LHV* is very low.

The pressure ratio β for the CH_4–H_2 mixture is slightly lower than for methane: this means that the compression station provides a lower pressure energy to the CH_4–H_2 mixture working fluid. Furthermore, the pressure ratio for biogas, which allowed the lowest energy delivery index Ψ values, is the highest.

Finally, the presence of a cooler along the main line (i.e. in ED1) is also evaluated. Fig. 6 shows that by using a cooler, of which the effect is simulated through a 10 °C decrease in compressor outlet temperature, the recycle valve is more closed, yet only very slightly. In fact, as outlined above, a lower temperature implies a higher density and, so, an increase in the protection margin of the anti-surge system is obtained.

4.2. Surge avoidance during emergency shutdown

The same PID-controlled recycle valve is used as a device for surge protection during an emergency shutdown. The emergency shutdown is simulated as follows: once the stationary condition is reached (at t = 150 s), the supplied power P_s is rapidly decreased towards zero in a trip time equal to 2 s.

Fig. 7 shows the operating lines for both fluids (black line for methane and gray line for biogas). The value for the *SM* imposed for the simulations is 20% for both fluids. The deceleration after emergency shutdown for methane cannot be observed in Fig. 7, since in practice it overlaps the deceleration curve for biogas. In Fig. 7, the stationary operating point *SOP* is also highlighted: the imposed emergency shutdown is started from this point.

In the case of methane, it can be noticed that, for a given corrected rotational speed value, the operating points during shutdown are characterized by a lower pressure ratio than that of the operating points during start-up. This is due to the fact that volumes are small and the inertia of the pressure (i.e. the resistance to a given variation) is low compared to the shaft inertia.

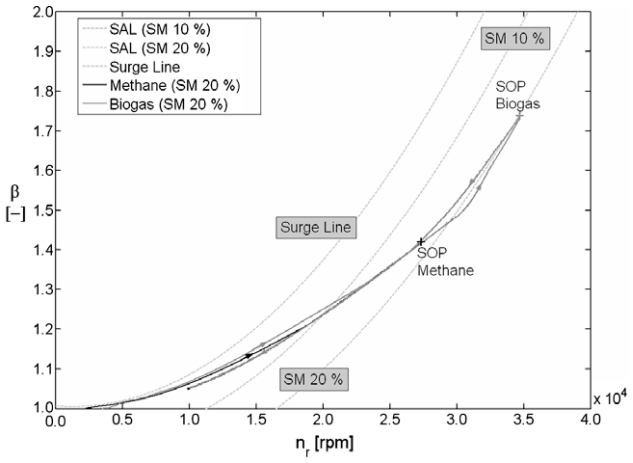

Fig. 7. Surge avoidance (emergency shutdown).

The same analysis is carried out for biogas as the operating fluid. In this case, the anti-surge system responds by increasing the valve coefficient when emergency shutdown occurs at t = 150 s, as shown in Fig. 8. Nevertheless, the surge margin is not ensured as shown in Fig. 7.

4.3. Surge avoidance during a change in the operating point

The considered change in the operating point consists of a rapid decrease of the outlet valve coefficient K_{Vout}, which passes from 5×10^{-3} m^2 to 2.5×10^{-3} m^2 in 5 s. This variation is imposed once the stationary condition is reached (at t = 150 s), as performed previously. This valve closure implies a lower mass flow rate at system delivery (Section 7 in Fig. 2).

The results are shown in Figs. 9 and 10. In the case of biogas as working fluid (gray line), the closure of the outlet valve leads the compressor to operate beyond the surge avoidance line transitorily. Then the recycle valve coefficient increases and a new stationary operating point, characterized by a lower corrected rotational speed and lower pressure ratio, is reached. Otherwise, in the case of methane (black line), the recycle system was not able to ensure the requested surge margin, even before outlet valve closure. So,

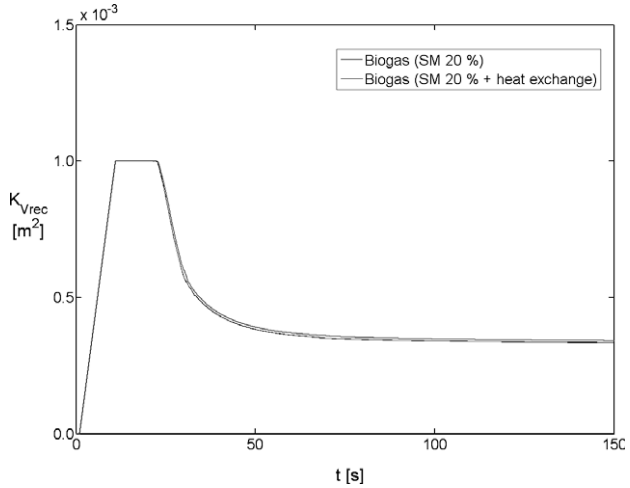

Fig. 6. Effect of the presence of a heat exchanger on recycle valve coefficient during start-up and normal operation.

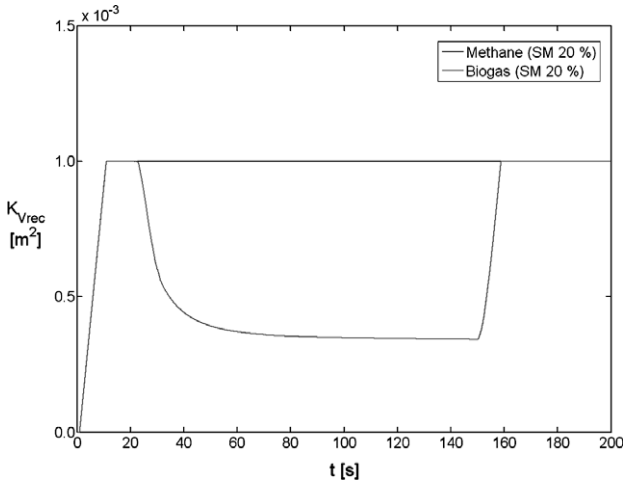

Fig. 8. Recycle valve coefficient (emergency shutdown).

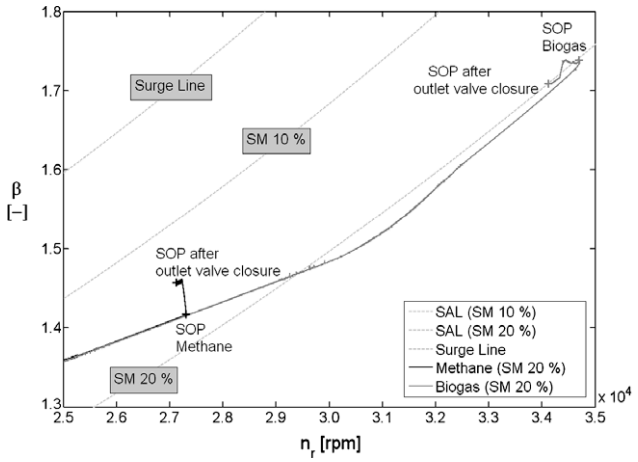

Fig. 9. Surge avoidance (change in operating point).

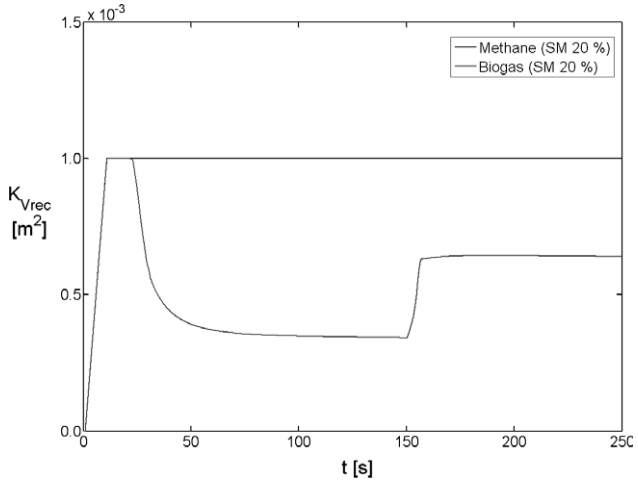

Fig. 10. Recycle valve coefficient (change in operating point).

when the outlet valve is closed, the compressor operating point moves towards higher pressure ratio and lower corrected rotational speeds.

4.4. Hot-gas by-pass system

The analyses which are carried out in this section refer to the case in which the recycle valve acts as a hot-gas by-pass [42]. In fact, the valve is closed during normal operation, while it rapidly opens in the case of an emergency shutdown.

Thus, two different options for driving the compressor are investigated separately:

- the compressor is driven by a gas turbine. So, the system is characterized by a long power trip time and low polar inertia;
- the compressor is driven by an electric motor, and so the system is characterized by fast trip and high inertia.

The trends of the supplied power P_s and of the recycle valve coefficient K_{Vacc} are shown in Fig. 11. The values of the characteristic times and of the inertia J for the two cases are resumed in Table 4.

As stated when dealing with the emergency shutdown maneuver, the inertia of pressures is low. Thus, in order to perform the

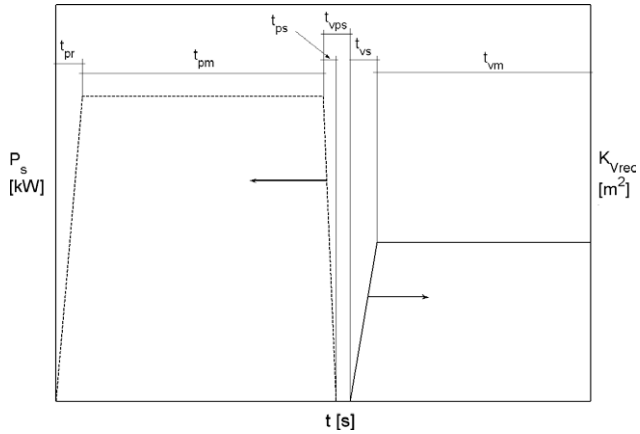

Fig. 11. Supplied power and recycle valve coefficient vs. time.

Table 4
Characteristic times and inertia for two compressor drivers.

		Gas turbine	Electric motor
t_{pr}	s	5	5
t_{pm}	s	95	195
t_{ps}	s	2	0.5
t_{vps}	s	0.1	0.1
t_{vs}	s	0.5	0.5
t_{vm}	s	49.4	99.4
J	kg m^2	0.1	0.5

Table 5
Model input parameters for hot-gas by-pass system analysis.

Property	Value	Unit	Ref.
Main line			
Hydraulic diameters, D_{hi} (i = 1,...,7)	0.25	m	
Intake duct length, L_{ID1}	600	m	
Intake duct length, L_{ID2}	1.5	m	
Exhaust duct length, L_{ED1}	19	m	
Exhaust duct length, L_{ED2}	600	m	
Compressor duct length, L_C	0.40	m	[44]
Friction factors λ_1, λ_3, λ_5, λ_7	0.05	–	
Access valve coefficient, $K_{Vacc} \times 10^3$	2.5	m^2	
Outlet valve coefficient, $K_{Vout} \times 10^3$	2.5	m^2	
Hot-gas by-pass line			
Hydraulic diameter, D_{hi} (i = 8,9)	0.04	m	[41]
Recycle duct length, L_{RD}	16	m	[41]
Friction factor, λ_8	0.01	–	
Maximum recycle valve coefficient, $K_{Vrec} \times 10^3$	2.5	m^2	
Ambient pressure, p_{amb}	101	kPa	
Ambient temperature, T_{amb}	15	°C	
Maximum power supplied, P_s	50	kW	

analyses of system behavior in the presence of a hot-gas by-pass, the configuration of the system under consideration is varied by increasing duct volumes. Moreover, in order to maintain a similar resistance behavior through the ducts, friction factors and valve coefficients are also changed. To do this, the former are increased, while the latter are decreased. The complete set of values of all model parameters is reported in Table 5.

Finally, it has to be underlined that the results reported in this section only refer to biogas, since system behavior with this fluid resulted less critical than with methane and consequently the different system response for the two compressor drivers can be highlighted.

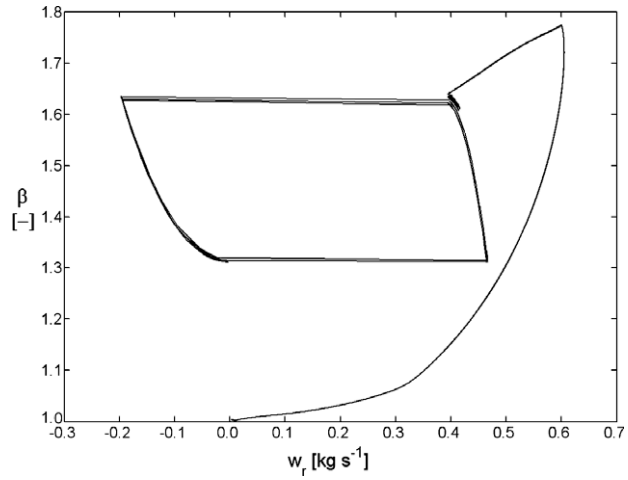

Fig. 12. Surge cycles after a gas turbine trip (biogas).

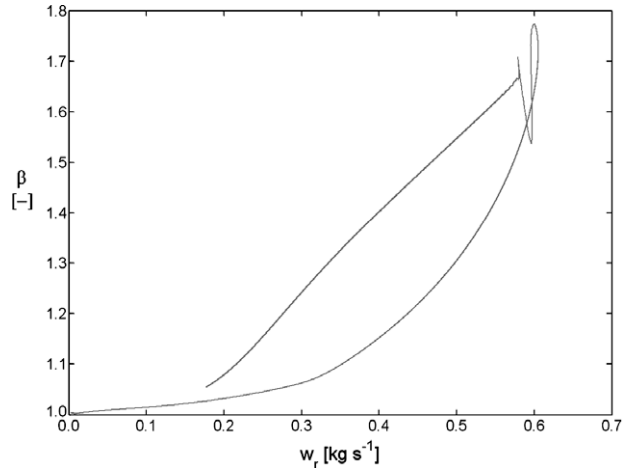

Fig. 13. Gas turbine trip in the presence of a hot-gas by-pass (biogas).

4.4.1. Gas turbine driven compressor

Fig. 12 shows the behavior of the compressor in the absence of the by-pass, which causes surge occurrence after gas turbine trip. The same maneuver in presence of the by-pass is represented in Fig. 13. It can be noticed that in this case the pressure ratio rapidly decreases and consequently surge does not occur.

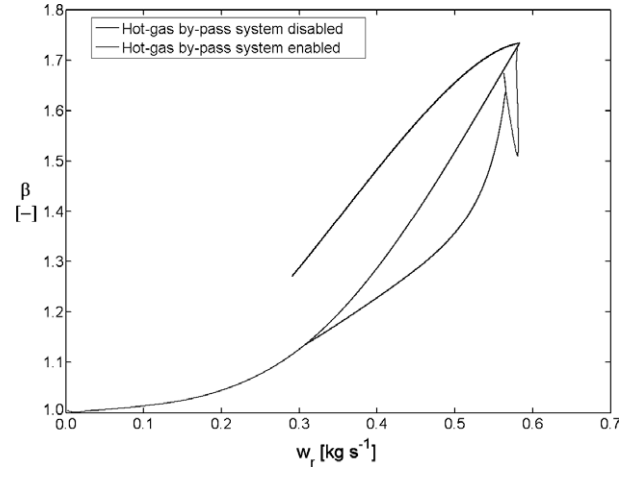

Fig. 14. Electric motor trip (biogas).

4.4.2. Electric motor driven compressor

In this case, the higher shaft inertia protects the compressor even though the trip is more rapid (0.5 s) than in the previous case (2 s), as shown in Fig. 14. In fact, the hot-gas by-pass is not necessary because surge does not occur even though the hot-gas by-pass is disabled. The effect of the presence of the by-pass is the same as in the previous case, i.e. to cause a rapid decrease in the pressure ratio.

5. Conclusions

In this paper, a non-linear one-dimensional modular dynamic model for the simulation of surge in compression systems was used to study a recycle line as a surge avoidance system.

The model provides a prediction of the behavior of the system during start-up, normal operation and emergency shutdown.

The influence of three different working fluids was evaluated: pure methane, biogas (i.e. a mixture of methane and carbon dioxide representative of the gas obtainable by means of biochemical conversion processes) and a methane–hydrogen mixture. Simulations prove that the design of the surge protection system should consider the fluid to be elaborated. As a rule of thumb, for a given surge avoidance system, the lower the fluid density the lower the safe margin, i.e. the recycle valve should be more open in order to provide the same surge margin.

The presence of a cooler along the main line was also evaluated. The results show that the presence of a cooler increases the safe margin. This is due to the fact that fluid density increases through cooling and, so, the mass flow rate through the recycle valve increases.

Two different drivers for the compressor were considered: a gas turbine and an electric motor. The former is characterized by low inertia and long trip time, while the latter is characterized by higher inertia and shorter trip time. An interesting result was that surge occurrence in compression systems in the case of driver shutdown is strictly dependent on the ratio between system volumes and the inertia of the rotating masses. In fact, system predisposition to surge increases as this ratio also increases.

References

[1] Parikka M. Global biomass fuel resources. Biomass Bioenergy 2004;27:613–20.
[2] Akhmatov V, Knudsen H. Large penetration of wind and dispersed generation into Danish power grid. Electr Power Syst Res 2007;77:1228–38.
[3] Paatero JV, Lund PD. Effects of large-scale photovoltaic power integration on electricity distribution networks. Renew Energy 2007;32:216–34.
[4] Greitzer EM. Surge and rotating stall in axial flow compressor: part 1, theoretical compression system model. ASME J Eng Power 1976;98:190–8.
[5] Tavakoli S, Griffin I, Fleming P. An overview of compressor instabilities: basic concepts and control. In: Proceedings of the 16th IFAC international symposium on automatic control in aerospace; 2004.
[6] Vachtsevanos G, Kang H, Cheng J, Kim I. Detection and identification of axial flow compressor instabilities. AIAA J Guid Control Dynam 1992;15:1216–23.
[7] McKee RJ. An internal flow measurement that senses a pre-cursor to surge in centrifugal compressors. In: Proc. ASME Turbo Expo; 2006.
[8] Kang JS, Kang SH. Stall inception in a high-speed centrifugal compressor. In: Proc. ASME Turbo Expo; 2001.
[9] Ishida M, Sakaguchi D, Ueki H. Incipient rotating stall characteristics measured by semiconductor L2F and pressure transducer in vaneless diffuser of centrifugal blowers. In: Proc. ASME Turbo Expo; 2000.
[10] Kurz R, White RC. Surge avoidance in gas compression systems. ASME J Turbomach 2004;126:501–6.
[11] D'Andrea R, Behnken RL, Murray RM. Rotating stall control of an axial flow compressor using pulsed air injection. ASME J Turbomach 1997;119:742–52.
[12] Gravdahl JT, Egeland O. Compressor surge and rotating stall. Modeling and control. London: Springer-Verlag; 1999.
[13] Li Minghong, Zheng Qun. Wet compression system stability analysis. Part I – wet compression Moore Greitzer transient model. In: Proc. ASME Turbo Expo; 2004.

[14] Skoch GJ. Experimental investigation of centrifugal compressor stabilization techniques. NASA TM-2003-212599.
[15] Arnulfi GL, Giannattasio P, Micheli D, Pinamonti P. An innovative device for passive control of surge in industrial compression systems. ASME J Turbomach 2001;123:473–82.
[16] Mizuki S, Tsujita H, Hishinuma Y. Control of surge for centrifugal compression system by using a bouncing ball. In: Proc. ASME Turbo Expo; 2000.
[17] Moore FK, Greitzer EM. A theory of post-stall transients in axial compression systems: part I – development of equations. ASME J Eng Gas Turbines Power 1986;108:68–76.
[18] Fink DA, Cumpsty NA, Greitzer EM. Surge dynamics in a free-spool centrifugal compressor system. ASME J Turbomach 1992;114:321–32.
[19] Mansoux CA, Gysling DL, Setiawan JD, Paduano JD. Distributed nonlinear modeling and stability analysis of axial compressor stall and surge. In: Proc. of American control conference; 1994. p. 2305–16.
[20] McCaughan FE. Application of bifurcation theory to axial flow compressor instability. ASME J Turbomach 1989;111:426–33.
[21] McCaughan FE. Bifurcational analysis of axial flow compressor stability. SIAM J Appl Math 1990;50:1232–53.
[22] Hős C, Champneys A, Kullmann L. Bifurcational analysis of surge and rotating stall in the Moore–Greitzer compression system. IMA J Appl Math 2003;68:205–28.
[23] Vaidya U, Ananthkrishnan N, Walimbe V. Nonlinear control of surge and stall in axial flow compressor. In: Proc. of the 5th national conference on airbreathing engines and aerospace propulsion (NCABE 2000); 2000. p. 102–10.
[24] Humbert JS, Krener AJ. Dynamics and control of entrained Greitzer compressor models. Int J Control 1998;71:807–21.
[25] Protz M, Paduano JD. rotating stall and surge: alternate modeling and control concepts. In: Proc. of the 1997 international conference on control application; 1997. p. 866–73.
[26] Gravdahl JT. Modeling and control of surge and rotating stall in compressors. Ph.D. Thesis, Norwegian University of Science and Technology; 1998.
[27] Arnulfi GL, Giannattasio P, Giusto C, Massardo AF, Micheli D, Pinamonti P. Multistage centrifugal compressor surge analysis: part II – numerical simulation and dynamic control parameters evaluation. ASME J Turbomach 1998;121:312–20.
[28] Hale AA, Davis MW. Dynamic turbine engine compressor code DYNTECC – theory and capabilities. In: Proc. of 28th AIAA/SAE/ASME/ASEE joint propulsion conference and exhibit; 1992.
[29] Owen AK, Daugherty A, Garrard D, Reynolds HC, Wright RD. A parametric starting study of an axial–centrifugal gas turbine engine using a one-dimensional dynamic engine model and comparisons to experimental results: part I – model development and facility description. ASME J Eng Gas Turbines Power 1999;121:377–83.
[30] Owen AK, Daugherty A, Garrard D, Reynolds HC, Wright RD. A parametric starting study of an axial–centrifugal gas turbine engine using a one-dimensional dynamic engine model and comparisons to experimental results: part II – simulation calibration and trade-off study. ASME J Eng Gas Turbines Power 1999;121:384–93.
[31] Owen AK, Davis Jr MW. Modeling the dynamic behavior of an axial–centrifugal compression system. In: Proc. of 30th AIAA/ASME/SAE/ASEE joint propulsion conference; 1994.
[32] Cousins WT. The dynamics of stall and surge behavior in axialcentrifugal compressors. Ph.D. Thesis, Virginia Polytechnic Institute and State University;1996.
[33] Theotokatos G, Kyrtatos NP. Investigation of a large high-speed diesel engine transient behavior including compressor surging and emergency shutdown. ASME J Eng Gas Turb Power 2003;125:580–9.
[34] Theotokatos G, Kyrtatos NP. Diesel engine transient operation with turbocharger compressor surging. SAE paper 2001-01-1241.
[35] Schmitz MB, Fitzky G. Surge cycle of turbochargers: simulation and comparison to experiments. In: Proc. ASME Turbo Expo; 2004.
[36] Botha BW, du Toit B, Rousseau PG. Development of a mathematical compressor model to predict surge in a closed loop Brayton cycle. In: Proc. ASME Turbo Expo; 2003.
[37] Hahn A. Modeling and control of solid oxide fuel cell–gas turbine power plant systems. Ph.D. Thesis, University of Pittsburgh; 2000.
[38] Hildebrandt A, Genrup M, Assadi M. Steady-state and transient compressor surge behaviour within a SOFC-GT-hybrid system. In: Proc. ASME Turbo Expo; 2004.
[39] Botros KK, Campbell PJ, Mah DB. Dynamic simulation of compressor station operation including centrifugal compressor and gas turbine. ASME J Eng Gas Turbines Power 1991;113:300–11.
[40] Botros KK. Transient phenomena in compressor stations during surge. ASME J Eng Gas Turbines Power 1994;116:133–42.
[41] Botros KK, Jungowski WM, Richards DJ. Compressor station recycle system dynamics during emergency shutdown. ASME J Eng Gas Turbines Power 1996;118:641–53.
[42] Bakken LE, Bjørge T, Bradley TM, Smith N. Validation of compressor transient behavior. In: Proc. ASME Turbo Expo; 2002.
[43] Tveit GB, Bjørge T, Bakken LE. Impact of compressor protection system on rundown characteristics. In: Proc. ASME Turbo Expo; 2005.
[44] Morini M, Pinelli M, Venturini M. Development of a one-dimensional modular dynamic model for the simulation of surge in compression systems. ASME J Turbomach 2007;129:437–47.
[45] Venturini M. Development and experimental validation of a compressor dynamic model. ASME J Turbomach 2005;127:599–608.
[46] Šilhavỳ M. The mechanics and thermodynamics of continuous media. Berlin: Springer-Verlag; 1997.
[47] Koff SG, Greitzer EM. Axisymmetrically stalled flow performance for multistage axial compressors. ASME J Turbomach 1986;108:216–23.
[48] Cumpsty NA. Compressor aerodynamics. Harlow: Longman Scientific and Technical; 1989.
[49] Astrom K, Hagglund T. PID controllers: theory, design, and tuning. 2nd ed. Research Triangle Park: Instrument Society of America; 1995.
[50] Bettocchi R, Pinelli M, Spina PR, Venturini M, Cenci G, Morini M. Energy production from biomass: development of a general model and application to anaerobic digestion. In: Proc. ASME Turbo Expo; 2007.
[51] Florisson O, Alliat I, Lowesmith B. The value of the existing natural gas system for hydrogen, the sustainable future energy carrier (progress obtained in the NATURALHY-project). In: Proceedings of the 23rd world gas conference; 2006.